NANO LETTERS

LETTER

pubs.acs.org/NanoLett

From Two-Dimensional Colloidal Self-Assembly to Three-Dimensional Nanolithography

C.-H. Chang,*[,†] L. Tian,[†] W. R. Hesse,[†] H. Gao,[‡] H. J. Choi,[†] J.-G. Kim,[†] M. Siddiqui,[†] and G. Barbastathis[†,§]

[†]Department of Mechanical Engineering and [‡]Department of Electrical Engineering and Computer Science, Massachusetts Institute of Technology, Cambridge, Massachusetts 02139, United States

[§]Singapore-MIT Alliance for Research and Technology (SMART) Centre, Singapore

Supporting Information

ABSTRACT: A number of "top-down" lithographic and "bottom-up" self-assembly methods have been developed to fabricate three-dimensional (3D) nanostructures to support the recent advances in nanotechnology. But they are limited by a number of factors such as fabrication cost, pattern resolution, and/or flexibility of geometry. Here we present a 3D nanolithography process that utilizes self-assembled nanospheres to create a periodic array of focal spots, which are then replicated across multiple depth in a transparent medium according to the Talbot effect. The Talbot field then exposes a pattern onto the underlying photoresist, recording the 3D intensity distribution. We have demonstrated designable complex 3D periodic structures with 80 nm minimum feature size, roughly one-fourth of the operating wavelength. This approach combines 2D colloidal self-assembly and 3D phase lithography, is robust, cost-effective, and widely applicable to nanoscale research and manufacturing.

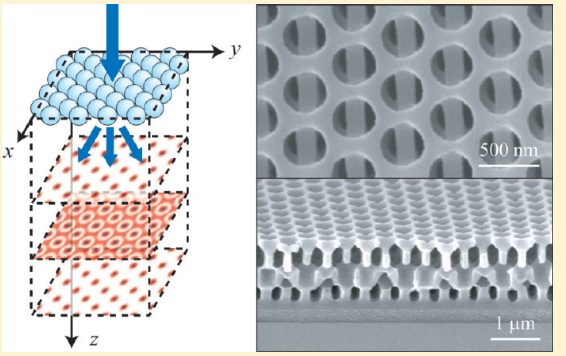

KEYWORDS: 3D nanostructures, colloidal assembly, nanosphere lithography, phase lithography

In recent years, advances in fabrication of periodic three-dimensional (3D) nanostructures have enabled a number of key innovations in nanoscience, such as photonic[1−3] and phononic crystals,[4] micro/nano frames,[5] and nanoporous filters.[6] One attractive method is phase-shift lithography,[6−9] where a 2D phase mask is illuminated to generate a 3D intensity distribution. The photoresist, typically placed in direct contact, records the intensity to form 3D nanostructures. However, in this method it is essential to use high quality nanostructured phase masks, which generally require expensive and complex processes such as deep-ultraviolet (UV),[6] interference,[7] Dip-Pen,[8] and electron-beam lithography.[9]

In addition to the "top-down" phase lithography approach, colloidal self-assembly has also been demonstrated as a viable "bottom-up" nanofabrication technique.[10−18] In this method monodispersed micro/nanospheres are dispersed to form 2D hexagonal close-packed structures due to interparticle capillary forces. These 2D patterns can then be used as a physical mask for subsequent additive deposition[10,11,14] or subtractive etching processes.[13−15] Colloidal assembly can also be extended to form 3D nanostructures;[12,16,17] however, the assembled structure suffers from long settling time, limited lattice geometry, and lattice defects.

Here we introduce an alternative phase-shift lithography approach that can be used to pattern 3D nanostructures with designable lattice period. In this approach, the physical mask is replaced by an array of self-assembled colloidal nanospheres. The array functions as a phase element and generates a 3D intensity distribution when illuminated. Each sphere focuses the normal-incident beam, behaving as a "colloidal ball lens." The spheres can be assembled directly on the photoresist, effectively integrating the phase element on the substrate. The proposed process thus does not require a physical mask, eliminating mask fabrication cost and reducing process complexity. Eliminating the physical mask also circumvents close-contact issues such as particle contamination, gap nonuniformity, and mask distortion. Furthermore, since only a monolayer of nanospheres is required, the number of defects can be less than assembly over a 3D volume. There has been exciting work in using submicrometer spheres for subwavelength nanolithography[19,20] and surface ablation,[21] but these have all been limited to 2D geometries. To the best of our knowledge, we are the first to successfully fabricate 3D structures by harnessing the volumetric nature of the intensity distribution.

The proposed process is illustrated in Figure 1, where a monolayer of nanospheres with diameter D is assembled on the substrate and illuminated with normal incident light. Since the sphere assembly is periodic, the light diffracted past it will exhibit the Talbot effect,[22] resulting in intensity patterns that repeat with an axial period z_t along the propagation distance z.

Received: April 8, 2011
Revised: May 2, 2011
Published: May 13, 2011

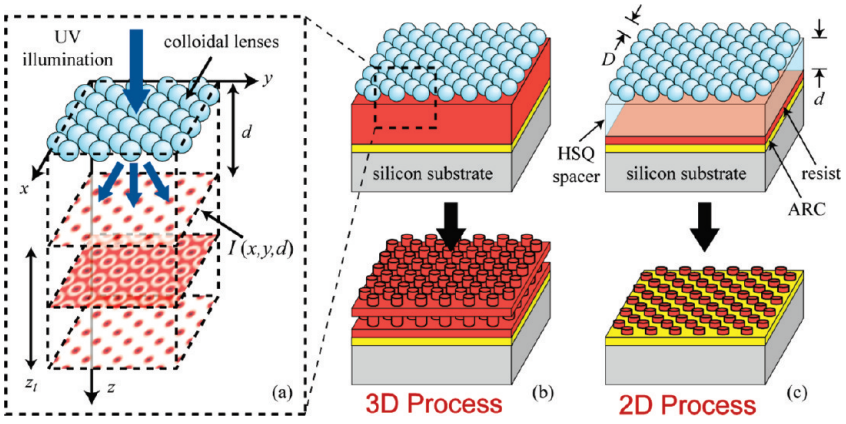

Figure 1. (a) Schematic of the proposed approach, where a hexagonal array of nanospheres is illuminated by a UV laser to generate a 3D intensity distribution. The $x-y$ intensity pattern is a function of propagation distance d. (b) The volumetric intensity distribution can be recorded by assembling the nanospheres directly on a substrate spincoated with thick photoresist. (c) A thin photoresist layer can also be used to capture a single 2D plane of the intensity distribution. The patterned geometry can be controlled by using a spacer layer to design the propagation distance d to the photoresist.

The Talbot distance, is given by

$$z_t = \frac{\frac{\lambda}{n}}{1 - \sqrt{1 - \left(\frac{\lambda}{n\Lambda}\right)^2}}$$

where λ and n are the incident wavelength and index of propagating medium, respectively, and for the hexagonal array of spheres $\Lambda = D(3)^{1/2}/2$ is the lateral period (for derivation see Supporting Information A). Note this expression simplifies to the more well-known equation $z_t = 3D^2/2\lambda$, for $D \gg \lambda$.[22] While the lateral period Λ depends on the sphere diameter, the axial period z_t can be designed by specifying $\gamma = \lambda/n\Lambda$.

We propose two fabrication processes to pattern 3D structures by using thick photoresist, as shown in Figure 1b, and 2D structures by using a transparent hydrogen silsesquioxane (HSQ) spacer layer to control the propagation distance to a thin resist layer, as shown in Figure 1c. The purpose of the latter is to fabricate structures that are more complex than the initial assembly geometry.

In all experiments, the samples were prepared on silicon substrates. A 300 nm thick antireflection coating (ARC, Brewer Science BARLi) layer was used to reduce back reflection. For the 3D and 2D samples, 1−1.5 μm and 60 nm of photoresist (Sumitomo PFi88A8) were spincoated on the ARC layer, respectively. For the 2D samples, a thin layer (15 nm) of silicon oxide was deposited using electron-beam evaporation on the thin resist before spincoating HSQ (Dow Corning FOX-16) to the desired spacer thickness. The HSQ film was baked at relatively low temperature of 95 °C for 1 min due to underlying photoresist. To enhance sphere adhesion, 15 nm silicon oxide was deposited on top of photoresist for both samples. See Supporting Information D for detailed stack diagram and material properties. Monodispersed polystyrene spheres with various diameters (Polyscience Polybead Microspheres in 2.5% aqueous solution) were used in our experiments. The solution was dispensed on the prepared substrate and allowed to dry in atmosphere.

The lithographic exposure was conducted using either a HeCd laser (λ = 325 nm), an Ar ion laser (λ = 351.1 nm), or a narrowband filtered mercury lamp centered at 405 nm. The 2D samples were exposure with dose of 50−60 mJ/cm^2, while the 3D samples with thick photoresist were exposed with higher doses of 100−200 mJ/cm^2. After exposure the nanospheres were removed by rinsing in acetone, isopropanol, and water. The thin layer of silicon oxide, as well as the HSQ spacer layer for the 2D samples, were etched using buffered hydrofluoric acid (Transene Company, Buffered HF Improved). The exposed photoresist was developed in 2.4% tetramethylammonium hydroxide (TMAH) aqueous solution (Microposit CD 26) for 1−2 min under ultrasonic agitation.

The 2D samples are fabricated using 450 nm diameter spheres and exposed with λ = 325 nm light, as shown in Figure 2. A cross-section view of the exposure condition is depicted in Figure 2a, overlaid with the optical intensity profile calculated using finite-difference time-domain (FDTD) method.[23] The top-view diagram of the sphere array geometry is depicted in Figure 2b. It can be observed that the $x-y$ intensity pattern varies as a function of z. The simulated intensity distribution has z_t of 1200 nm, and complex profiles can be observed within a single period. Figure 2c−g are top-view scanning electron micrograph (SEM) images of samples with HSQ thicknesses of 40, 260, 500, 560, and 650 nm, respectively. The corresponding locations of each plane are labeled in the cross-section intensity profile shown in Figure 2a.

Several interesting characteristics of the Talbot effect can be observed. First is the self-imaging pattern immediately below the sphere array (and also at integer multiples of z_t), where the structure replicates the original hexagonal hole array, as shown in Figure 2c. At roughly $z_t/2$ the image-reversed pattern, hexagonal array of dots, can be fabricated, as shown in Figure 2e. A spatial-frequency multiplied subpattern is observed in Figure 2d, where the lateral period of the fabricated structure is $D/(3)^{1/2}$ and the lattice is rotated by 30°. It is also possible to fabricate a hexagonal array of rings, as shown in Figure 2g. The width of the rings are ~90 nm, roughly $\lambda/4$. Note that the subwavelength pattern is possible due to solid immersion in the photoresist.

The fabrication results from four 3D samples with various axial period z_t are illustrated in Figure 3. The exposure parameters are given in the caption. Micrographs of Sample I from different views are shown in Figure 3a−d, and z_t is measured to be 750 nm. The cross-section micrographs of the structure are shown in Figure 3a,b, where defect-free 3D nanostructures can be obtained

dx.doi.org/10.1021/nl2011824 |*Nano Lett.* 2011, 11, 2533–2537

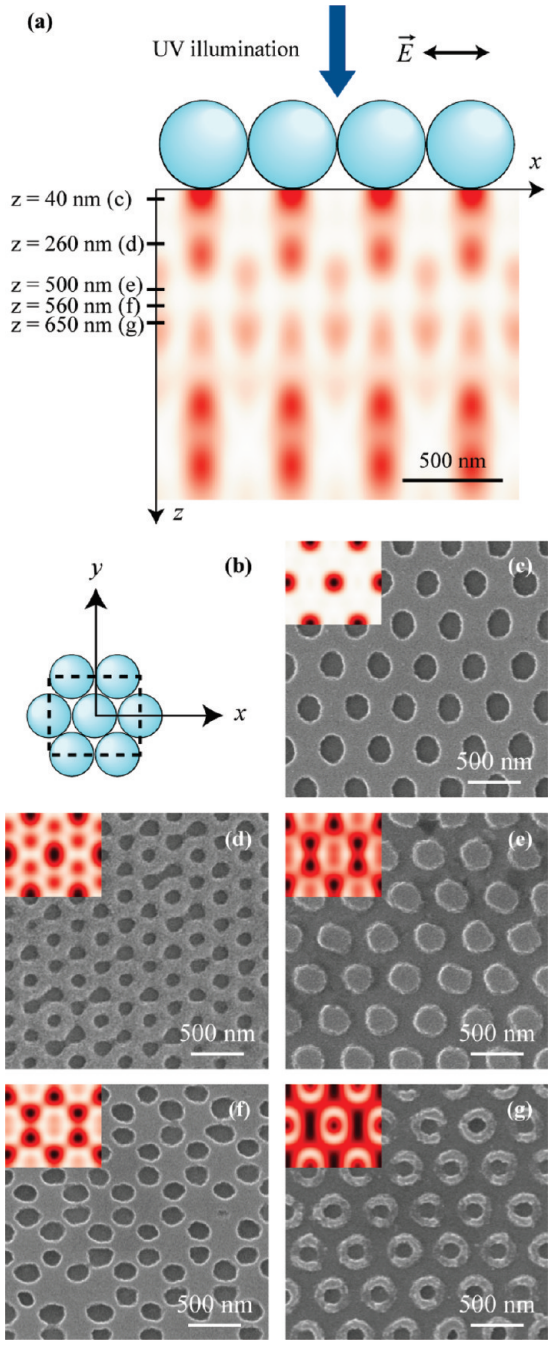

Figure 2. (a) Schematic of cross-section view during exposure, overlaid with intensity profile simulated using FDTD. A number of *z*-planes with designed propagation distances are marked and their corresponding fabrication results are shown in (c−g). The incident light is polarized in the *x*-direction. (b) Top-view diagram of assembled colloidal lens geometry. The same axes are used in (c−g). Top-view micrograph of fabricated structures with spacer thickness of (c) 40, (d) 260, (e) 500, (f) 560, and (g) 650 nm. The inset diagrams are simulated intensity profile for each plane.

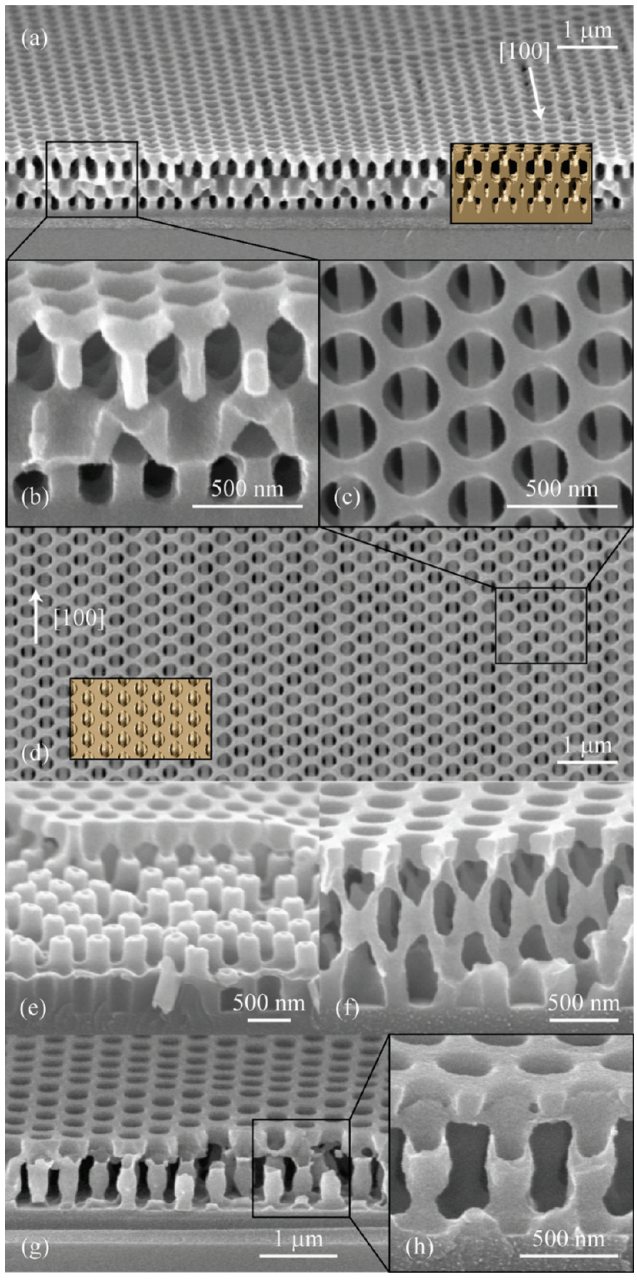

Figure 3. Micrographs of fabricated nanostructure with (a−d) λ = 351 nm, D = 350 nm, and γ = 0.67, (e) λ = 405 nm, D = 450 nm and γ = 0.63, (f) λ = 351 nm, D = 450 nm, and γ = 0.52, and (g−h) λ = 325 nm, D = 450 nm, and γ = 0.47. (a−d) The structure contains alternating 2D hexagonal holes array and 1D grating lines due to laser polarization. (e) The structure is exposed using unpolarized light, where the polarization effect is not observed. (f) The larger D and high γ ratio resulted in structure with shorter z_t. (g,h) The exposure condition has γ less than $1/(3)^{1/2}$, resulting in more complex geometry. The structure is vaselike and consists of a hollow core and solid base.

over ~100 μm^2 area. The patterned structure has alternating layers of hexagonal hole array and grating lines. A higher-magnification micrograph of the cross-section geometry is shown in Figure 3b, where the grating lines are oriented into the image. The grating layer can be better observed in the top-view micrographs of the same sample shown in Figure 3c,d. This result is due to the use of polarized light, which leads to 2-fold symmetry (see Supporting Information B). This effect is not seen in Sample II (Figure 3e), where the sample was exposed with nonpolarized, narrowband-filtered mercury lamp to retain the 6-fold symmetry of the sphere array. It is also important to note that the proposed method does not require highly coherent laser sources.

dx.doi.org/10.1021/nl2011824 |*Nano Lett.* 2011, 11, 2533–2537

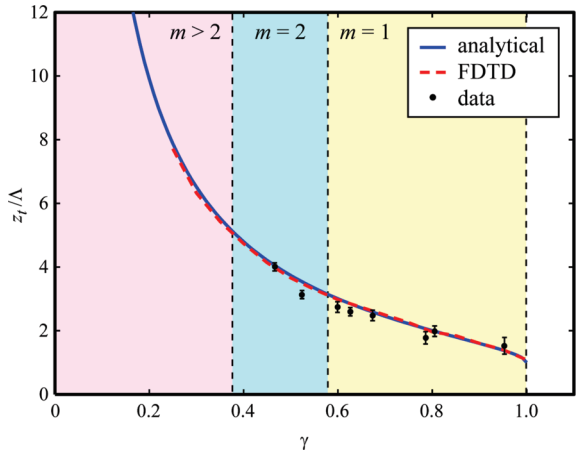

Figure 4. Plot of normalized axial period as a function of $\gamma = \lambda/n\Lambda$. The solid and dashed lines represent the analytical and FDTD numerical models. The data points are experimentally measured z_t in the fabricated structures. The colored area denote the regions where m diffraction orders are allowed to propagate in the photoresist. The boundaries are given by $\gamma = 1/(3)^{1/2}$ and $1/(7)^{1/2}$.

Sample III and IV are shown in Figure 3f and 3g,h, respectively, with z_t measured to be 1220 and 1560 nm, respectively. Under the hexagonal hole array, the fabricated structures in Sample IV resemble a vaselike geometry, each with hollow core and solid base. The hollow core was also observed as hexagonal array of rings in the planar fabrication results, depicted in Figure 2e. The structure geometry of Sample IV is more complex because the lower γ ratio allow for higher order diffracted beam to propagate into the photoresist layer (see Supporting Information A). In these experiments the structure height was limited to ~1.3 μm because the photoresist used absorbs at the exposure wavelength. Mechanical stability of the polymer material is also a limiting factor, degrading rapidly as the porous 3D structure increases in height. Taller structures can be fabricated by using more transparent and rigid materials such as SU-8[6,7] and is currently under investigation.

As we have demonstrated, the axial period of the fabricated structure can be controlled by selecting the appropriate γ ratio. Experimental verification of the dependency of normalized z_t/Λ on γ is illustrated in Figure 4, where the fabricated results are compared to analytical and numerical (FDTD) calculations (for detailed description see Supporting Information C). In theory, z_t/Λ has a lower limit of 1 at which point no diffraction orders can be observed in the photoresist. The colored background outlines the regime where m orders are allowed to propagate, and more interfering orders result in increased complexity of the Talbot pattern. The good agreement demonstrates that tuning the axial period and complexity of the 3D structure can be achieved by selecting the appropriate γ ratio.

One limitation of the colloidal approach is defects in the assembled 2D sphere array. This becomes increasingly problematic when using nanospheres with smaller diameters (D < 300 nm) due to wider size distribution. The assembled sphere array is therefore not perfectly periodic, and leads to incoherent scattering in the Talbot field generated (see Supporting Information C). A potential method to reduce defect density is to assemble the sphere in templates, which have demonstrated defect-free area over ~1 cm^2.[12] It is also interesting to note that while in this work the sphere array used have been limited to monolayers, it is possible to utilize multiple layers or co-self-assembly of spheres with different sizes[18] to generate more complex Talbot field patterns.

In this work, we have fabricated complex 3D nanostructures by harnessing the Talbot field distribution generated by a 2D nanosphere array. The pattern formation mechanism is analogous to phase-mask lithography, but in this case self-assembled nanospheres are employed as an integrated phase element. This approach eliminates mask fabrication costs and avoids close-contact issues. The proposed process combines 2D self-assembly with 3D nanolithography, exploring the advantages of both top-down and bottom-up approaches. This general fabrication concept can be implemented as a novel technique to fabricate complex 3D nanostructures in all fields of nanoscale research.

■ ASSOCIATED CONTENT

Supporting Information. Additional information and figures. This material is available free of charge via the Internet at http://pubs.acs.org.

■ AUTHOR INFORMATION

Corresponding Author
*E-mail: chichang@mit.edu.

■ ACKNOWLEDGMENT

We gratefully acknowledge the students, staff, and facility support from the 3D Optical Systems Group, Space Nanotechnology Laboratory, NanoStructures Laboratory, Quantum Nanostructures and Nanofabrication Group, and Microsystems Technology Laboratory at MIT. This research was funded by the Singapore National Research Foundation (NRF) through the Singapore-MIT Alliance for Research and Technology (SMART) Centre, the U.S. Air Force Office of Scientific Research (AFOSR) through the MURI program (Contract FA9550-08-1-0379), the U.S. Army Research Office (ARO) through the Institute for Soldier Nanotechnology (ISN) at MIT, and DOD NDSEG and NSF GRF (grant 0645960) fellowships.

■ REFERENCES

(1) Lin, S. Y.; Fleming, J. G.; Hetherington, D. L.; Smith, B. K.; Biswas, R.; Ho, K. M.; Sigalas, M. M.; Zubrzycki, W.; Kurtz, S. R.; Bur, Jim A three-dimensional photonic crystal operating at infrared wavelengths. *Nature* **1998**, *394*, 251–253.

(2) Noda, S.; Tomoda, K.; Yamamoto, N.; Chutinan, A. Full three-dimensional photonic bandgap crystals at near-infrared wavelengths. *Science* **2000**, *289*, 604–606.

(3) Mei, D.; Cheng, B.; Hu, W.; Li, Z.; Zhang, D. Three-dimensional ordered patterns by light interference. *Opt. Lett.* **1995**, *20* (5), 429–431.

(4) Gorishnyy, T.; Ullal, C. K.; Maldovan, M.; Fytas, G.; Thomas, E. L. Hypersonic Phononic Crystals. *Phys. Rev. Lett.* **2005**, *94*, 115501.

(5) Jang, J.-H.; Ullal, C. K.; Choi, T.; Lemieux, M. C.; Tsukruk, V. V.; Thomas, E. L. 3D Polymer Microframes That Exploit Length-Scale-Dependent Mechanical Behavior. *Adv. Mater.* **2006**, *18*, 2123–2127.

(6) Jeon, S.; Park, J.-U.; Cirelli, R.; Yang, S.; Heitzman, C. E.; Braun, P. V.; Kenis, P. J. A.; Rogers, J. A. Fabricating complex three-dimensional nanostructures with high-resolution conformable phase masks. *Proc. Natl. Acad. Sci. U.S.A.* **2004**, *101* (34), 12428–12433.

(7) Jang, J.-H.; Ullal, C. K.; Maldovan, M.; Gorishnyy, T.; Kooi, S.; Koh, C.; Thomas, E. L. 3D micro- and nanostructures via interference lithography. *Adv. Funct. Mater.* **2007**, *17*, 3027–3041.

(8) Jang, J.-W.; Zheng, Z.; Lee, O.-S.; Shim, W.; Zheng, G.; Schatz, G. C.; Mirkin, C. A. Arrays of nanoscale lenses for subwavelength optical lithography. *Nano Lett.* **2010**, *10* (11), 4399–4404.

(9) Isoyan, A.; Jiang, F.; Cheng, Y. C.; Cerrina, F.; Wachulak, P.; Urbanski, L.; Rocca, J.; Menoni, C.; Marconi, M. Talbot lithography: self-imaging of complex structures. *J. Vac. Sci. Technol., B* **2009**, *27* (6), 2931–2937.

(10) Hulteen, J. C.; Van Duyne, R. P. Nanosphere lithography: A materials general fabrication process for periodic particle array surfaces. *J. Vac. Sci. Technol., A.* **1995**, *13*, 1553–1558.

(11) Rybczynski, J.; Ebels, U.; Giersig, M. Large-scale, 2D arrays of magnetic nanoparticles. *Colloids Surf., A* **2003**, *219*, 1–6.

(12) Xia, Y.; Gates, B.; Yin, Y.; Lu, Y. Monodispersed colloidal spheres: old materials with new applications. *Adv. Mater.* **2000**, *12* (10), 693–713.

(13) Haginoya, C.; Ishibashi, M.; Koike, K. Nanostructure array fabrication with a size-controllable natural lithography. *Appl. Phys. Lett.* **1997**, *71* (20), 2934–2936.

(14) Yang, S.-M.; Jang, S. G.; Choi, D.-G.; Kim, S.; Yu, H. K. Nanomachining by colloidal lithography. *Small* **2006**, *2* (4), 458–475.

(15) Chen, H. L.; Chuang, S. Y.; Lin, C. H.; Lin, Y. H. Using colloidal lithography to fabricate and optimize sub-wavelength pyramidal and honeycomb structures in solar cells. *Opt. Express* **2007**, *15* (22), 14793–14803.

(16) van Blaaderen, A.; Rue, R.; Wiltzius, P. Template-directed colloidal crystallization. *Nature* **1997**, *385*, 321–324.

(17) Gates, B.; Qin, D.; Xia, Y. Assembly of nanoparticles into opaline structures over large areas. *Adv. Mater.* **1999**, *11* (6), 466–469.

(18) Yu, J.; Yan, Q.; Shen, D. Co-self-assembly of binary colloidal crystals at the air-water interface. *ACS Appl. Mater. Interfaces* **2010**, *2* (7), 1922–1926.

(19) McLeod, E.; Arnold, C. B. Subwavelength direct-write nanopatterning using optically trapped microspheres. *Nat. Nanotechnol.* **2008**, *3*, 413–416.

(20) Wu, W.; Katsnelson, A.; Memis, O. G.; Mohseni, H. A deep subwavelength process for the formation of highly uniform arrays of nanoholes and nanopillars. *Nanotechnology* **2007**, *18*, 485302.

(21) Lu, Y.; Chen, S. C. Nanopatterning of a silicon surface by near-field enhanced laser irradiation. *Nanotechnology* **2003**, *14*, 505–508.

(22) Winthrop, J. T.; Worthington, C. R. Theory of Fresnel images. I. plane periodic objects in monochromatic light. *J. Opt. Soc. Am.* **1965**, *55* (4), 373–381.

(23) Oskooi, A. F.; Roundy, D.; Ibanescu, M.; Bermel, P.; Joannopoulos, J. D.; Johnson, S. G. MEEP: A flexible free-software package for electromagnetic simulations by the FDTD method. *Comput. Phys. Commun.* **2010**, *181*, 687–702.